Rapid Post-Wildfire Burned Vegetation Assessment with Google Earth Engine (Case Study: 2023 Canada Wildfires)

Behnam Ebadati [1], Mohammad Alikhani [2], Fahimeh Youssefi [3], Saied Pirasteh[3]

[1] Dept. of Geomatic Engineering, South Tehran Branch, Islamic Azad University, Tehran, Iran - st_b_ebadati@azad.ac.ir
[2] Geodesy and Geomatics Engineering Faculty, K. N. Toosi University of Technology, Tehran, Iran - m.alikhani1@email.kntu.ac.ir
[3] Institute of Artificial Intelligence, Shaoxing University, 508 West Huancheng Road, Yuecheng District, Shaoxing, Zhejiang Province, Postal Code 312000, China - youssefi@usx.edu.cn, sapirasteh1@usx.edu.cn

Keywords: Burned Vegetation, Burn Severity, Wildfire, Machine Learning, Decision Level Fusion, Sentinel-2.

Abstract

Wildfires are significant environmental threats, requiring precise and prompt assessment to mitigate damage and guide recovery efforts. Remote sensing, mainly through satellite imagery multispectral data, provides practical tools for monitoring and evaluating wildfire impacts. Canada experiences significant wildfires each year, causing substantial damage to the country's environment, particularly its vegetation. This study proposed a fast and efficient method using Google Earth Engine (GEE) cloud-based computing to rapidly assess burned vegetation following a wildfire in Canada in 2023, utilizing Sentinel-2 imagery data. This method computed NDVI, GNDVI, and EVI spectral indices for classifying pre-fire vegetation cover and NBR, dNBR, and MIRBI for classifying post-fire burn severity. These spectral indices served as input data for machine learning models, including K-Nearest Neighbors (KNN), Random Forest (RF), Gradient Boosting Decision Trees (GBDT), and Support Vector Machine (SVM). Ultimately, the results of vegetation cover and burn severity classifications, performed separately by these models, were combined using a decision-level fusion with a weighting approach based on an accuracy approach to produce integrated and final classifications. Subsequently, by overlapping the results of these fused classifications, the burned vegetation was assessed, and its area was estimated. According to the study's results, significant damage was observed in the vegetation after the wildfire. 4489 km^2 of the study area, which was a Military Grid Reference System (MGRS) tile with an area of 12,000 km^2, was burned due to the wildfire. 34.06% of this area was specifically burned vegetation, equating to approximately 4,088 km^2.

1. Introduction

Wildfires, along with other common natural disasters such as floods, earthquakes, and droughts, continuously occur across various regions of the world (Seydi et al., 2021). The frequency of these destructive events, driven by climate change, has significantly increased, surpassing nature's capacity to mitigate their negative impacts (Sobrino et al., 2019). In addition to potential loss of life, wildfires can disrupt the ecological balance, cause soil erosion, destroy wildlife habitats, increase future flood risks (Chuvieco et al., 2020), degrade vegetation quality, reduce soil moisture (Soverel et al., 2010), and contribute to global warming through the release of carbon dioxide and methane gases (Srivastava and Senthil Kumar, 2020). Furthermore, wildfires are recognized as one of the primary disruptors of vegetation phenology (Wang and Zhang, 2020). Long-term wildfires, in particular, can significantly impact and damage large portions of vegetation, especially forests (Priya and Vani, 2024). For instance, a recent wildfire in 2021 destroyed approximately 400 km^2 of forests in northern Evia Island, Greece (Gemitzi and Koutsias, 2022). These factors have made wildfires an increasing concern for humans and the environment (Salvoldi et al., 2020). Therefore, acquiring the necessary information and mapping burned areas, particularly assessing the damage to vegetation following a wildfire event, is crucial. Remote sensing techniques are far more efficient than traditional methods for examining burned areas and assessing wildfire damage. Although traditional methods may offer higher accuracy, they are often limited by high costs and time consumption. Remote sensing overcomes these limitations by covering large surface areas and providing essential information for monitoring and managing natural disasters (Seydi et al., 2021; Priya and Vani, 2024; Pérez-Cabello et al., 2022; Izadi et al., 2017). Many researchers have confirmed remote sensing data's use and practical application in wildfire-related studies (Aksoy et al., 2023; Amos and Ferentinos, 2019; Huot et al., 2022; Ismailoglu and Musaoglu, 2023; Kulinan et al., 2024; Leblon, 2001; Lee et al., 2024). These studies utilize diverse optical, thermal, radar, and LIDAR sensors (Vandansambuu et al., 2023).

Among the open-access satellite imagery data, such as Sentinel-2, Landsat series, and MODIS data (Mandanici and Bitelli, 2016; Song et al., 2021), Sentinel-2 data offers significantly higher spatial and temporal resolution compared to Landsat series data (Claverie et al., 2018). Sentinel-2 mission provides researchers with excellent potential for examining burned areas and monitoring wildfires (Gibson et al., 2020; Seydi et al., 2021). Additionally, its spatial resolution is much higher than that of MODIS. However, with an almost daily temporal resolution, MODIS data can be more practical for monitoring post-wildfire vegetation phenology and seasonal changes in large areas (Pérez et al., 2022). Freely available remote sensing data from the GEE data catalog is accessed and processed through the platform, which simplifies remote sensing data processing via cloud-based computing, eliminating the need for personal hardware (Brovelli et al., 2020). The GEE applications are expanding across multiple research fields, including disaster management (Mutanga and Kumar, 2019). Various methods are commonly employed to assess burned areas and wildfire-induced damage using remote sensing data. Some of these methods focus primarily on classification techniques (Palandjian et al., 2009), while others utilize Principal Component Analysis (Hudak and Brockett, 2004) and can be effective in this context. Additionally, many methods for mapping burned areas rely directly or indirectly on spectral indices as complementary approaches (Bastarrika et al., 2011; Loboda et al., 2007). Spectral indices are more common due to their operational simplicity and higher efficiency than other methods (Veraverbeke et al., 2011). Spectral indices are essential for understanding surface processes. They are derived from various combinations of spectral bands. Previous research

has explored many applications for these indices across diverse fields, such as agriculture, water resource management, urban development, forest ecology, vegetation analysis, etc (Prasad et al., 2022). Wildfire impacts can be detected utilizing spectral indices sensitive to Red, Shortwave-Infrared (SWIR), and Near-Infrared (NIR) bands. These indices effectively assess burned vegetation (Fassnacht et al., 2021; Petropoulos et al., 2014). For example, the simple Normalized Burn Ratio (NBR) index can be cited as a widely used example with extensive applications in various related studies (Veraverbeke et al., 2010; French et al., 2008). Although spectral indices, due to their simple and understandable computational structure, can effectively address needs in analyzing various phenomena and features on the earth's surface, they cannot always be relied upon exclusively. Therefore, more advanced methods are required that not only leverage the effectiveness of these indices but also offer greater generalizability across different conditions. In this context, machine learning methods have increasingly gained attention. In recent years, numerous studies have been conducted using spectral indices derived from various spectral bands and machine-learning methods. Many of these studies have utilized cloud-based computing technologies such as Google Earth Engine (GEE) and Colab as effective tools for data access and open-source processing.

For instance, a study proposed an automated approach for global burned area mapping in 2015 using Landsat 8 data. This method utilized spectral indices and a Random Forest algorithm for the burned pixels detection, and after applying several filters, the final burned area map was generated. The high correlation between the results of this method and similar existing products demonstrated its effectiveness (Long et al., 2019). In another study, the potentials of the GEE and Colab services were utilized simultaneously to Iran burned areas mapping across the entire Iran using Landsat 8 data. In this study, 13 spectral indices were calculated and, along with the 9 spectral bands, were used as input data for Neural Network and Random Forest classifiers. The results showed classification accuracies of 94% and 96%, respectively, demonstrating the effectiveness of the proposed approach in burned areas mapping (Gholamrezaie et al., 2022). In a similar study, various spectral indices derived from Sentinel-2 imagery bands were calculated within the GEE platform to assess burned areas following wildfires in northern Morocco. These indices, used in different combinations along with the original bands, were applied in a Random Forest classifier. Although some of these combinations did not yield satisfactory results in several regions and even led to decreased accuracy with the inclusion of additional spectral bands, combinations utilizing the dNBR index demonstrated remarkable accuracies of 96% and above (Badda et al., 2023).

This study aims to test the capability of rapidly assessing burned vegetation after the 2023 wildfires in Canada using Sentinel-2 multispectral data processed in the GEE cloud computing environment. Several spectral indices with different applications, detailed in the methodology section, were utilized as input data for K-Nearest Neighbors, Random Forest (RF), Gradient Boosting Decision Tree (GBDT), and Support Vector Machine (SVM) classifiers. The KNN is a non-parametric method for classifying data based on the proximity of new samples to existing training data. KNN assigns a new sample to the most common class among its k closest neighbors (Pacheco et al., 2021). RF is one of the most popular and widely used machine learning algorithms and is renowned for its effectiveness. An ensemble learning method utilizes many decision tree models to provide a final prediction. Models based on this algorithm have high accuracy in performing classification and regression tasks (Breiman, 2001). In contrast, The GBDT builds a strong predictive model by iteratively adding small decision trees, each aimed at correcting the errors of the previous ones. This process continues until maximum accuracy is achieved or a set number of iterations is reached (Rao et al., 2019). The SVM identifies the optimal hyperplane to separate two data classes by focusing on the closest data points, called support vectors. It handles large, complex datasets effectively, prevents overfitting, and offers flexibility in selecting similarity functions (Kalantar et al., 2020). All four algorithms are among the most well-known machine learning algorithms, whose advantages are utilized in classifications through a decision-level fusion approach to assessing burned vegetation.

2. Study Area

Canada emerged as the epicenter of wildfires in 2023. While significant fire seasons are common, the total burned area that year reached 15.0 million hectares (Jain et al., 2024), surpassing the annual average of 2.1 million hectares by over seven times and doubling the previous record of 6.7 million hectares set in 1989. Notably, the largest single fire covered 1.14 million hectares, exceeding the previous largest wildfire of 858,000 hectares in 1995 (Kolden et al., 2024). The 2023 wildfires in Canada were selected as a case study for this research to examine the damage inflicted on vegetation cover following the fires. This study focuses exclusively on a single Sentinel-2 imagery tile where a significant wildfire occurred, and only images from this specific tile, identified as 12VVM, are utilized. Each tile in the tiling system corresponds to a Military Grid Reference System (MGRS) based on UTM, covering an area of approximately 12,100 km² of the Earth's surface. The central coordinates of this tile are approximately 59.921°N latitude and -111.7763°W longitude. Tile 12VVM Images, used for the rapid post-wildfire assessment of burned vegetation, includes Fort Smith Town, situated in the southern Slave region within the northern half of this tile. The area covered by this tile's images primarily features natural surface characteristics such as soil, vegetation, rocky outcrops, and water bodies, with vegetation cover being a significant portion of the landscape.

3. Methodology

3.1 Data

This study utilized Sentinel-2 level-2A data from May 1, 2023, to November 1, 2023, encompassing pre-wildfire and post-wildfire. Sentinel-2 Multi-Spectral Instrument (MSI) data, available through the GEE data catalog, is widely used for both global and regional analyses due to its comprehensive 13 spectral bands providing 10-meter spatial resolution (Meer et al., 2014; Q. Wang et al., 2017), also with a high temporal resolution of approximately five days (Drusch et al., 2012). Most necessary preprocessing steps, such as atmospheric, radiometric, and geometric corrections, were conducted in GEE, and the preprocessed data are provided as ready-to-use products. From May 1, 2023, to November 1, 2023, 68 Sentinel-2 images from the 12VVM tile were available for this study. Only 11 images with the minimum cloud cover percentage were selected, and the rest were filtered out. A Median filter was applied to reduce noise and the impact of clouds, shadows, and thick smoke during and after the wildfire. Considering that the final assessment of this study is based on calculating the area of burned vegetation after the complete end of the wildfire and comparing it with the conditions before the wildfire, at least two images from pre-wildfire and post-wildfire were needed. By

applying the Median filter and reducing or eliminating the effects of noise, clouds, shadows, and smoke, pre-wildfire and post-wildfire composite images were obtained. Figure 1 shows these two composite images.

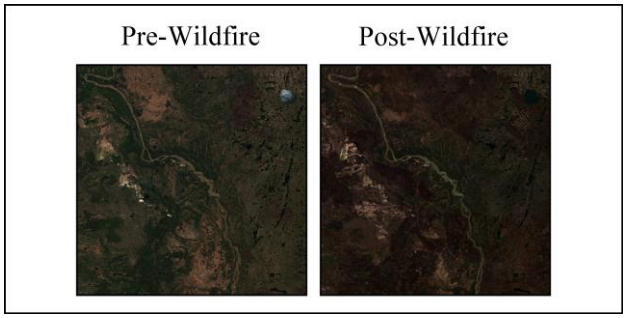

Figure 1. Pre-wildfire and post-wildfire composite images.

3.2 Spectral Indices

In this study, the Normalized Burn Ratio (NBR), differenced Normalized Burn Ratio (dNBR), and Mid-Infrared Burned Index (MIRBI) were computed to examine burned areas and burn severity classification. The Normalized Difference Vegetation Index (NDVI), Green Normalized Difference Vegetation Index (GNDVI), and Enhanced Vegetation Index (EVI) were computed to assess pre-wildfire vegetation cover. Also, the Normalized Difference Water Index (NDWI) was computed to extract water bodies such as rivers and small lakes in the study area.

Index	Equation	Reference
NBR	$\frac{NIR - SWIR}{NIR + SWIR}$	Lee et al., 2024
dNBR	$dNBR_{Pre-Fire} - dNBR_{Post-Fire}$	Lee et al., 2024
MIRBI	$10 \times SWIR_2 - 9.8 \times SWIR_1 + 2$	Zidane et al., 2021
NDVI	$\frac{NIR - Red}{NIR + Red}$	Huang et al., 2021
GNDVI	$\frac{NIR - Green}{NIR + Green}$	Espinoza et al., 2017
EVI	$2.5 \times \frac{(NIR - Red)}{(NIR + 6 - 7.5 \times Blue + 1)}$	Son et al., 2014
NDWI	$\frac{Green - NIR}{Green + NIR}$	Liu et al., 2024

Table 1. Spectral Indices

3.3 Random Samples

To speed up processing and avoid computational complexity due to the large number of pixels, not all pixel values from the calculated spectral indices are used as input data for training and testing in classification. Instead, a limited number of them are randomly selected as samples. Therefore, 1,000 random points were distributed across pre-wildfire and post-wildfire composite images. Figure 2 shows the distribution of these random points. The pixel values from these random points were used for training and testing the classification process as sample input data.

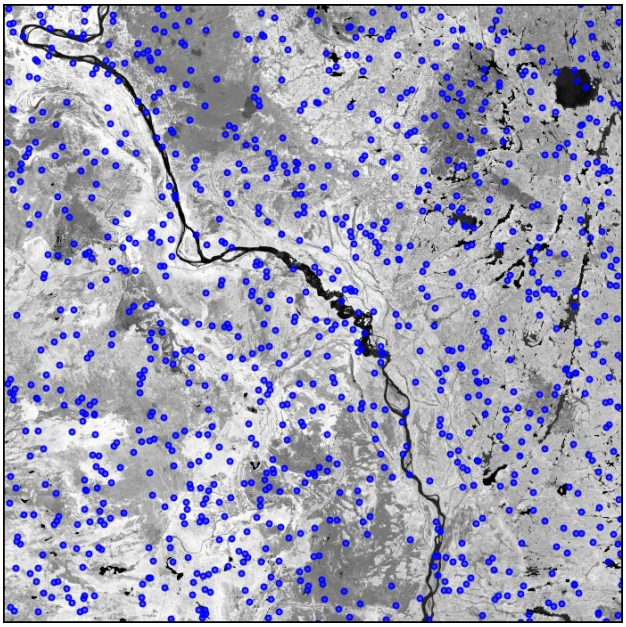

Figure 2. Random points dispersion in the study area.

3.4 Machine Learning Classifiers

This study employs K-Nearest Neighbor (KNN), Random Forest (RF), Gradient Boosting Decision Trees (GBDT), and Support Vector Machine (SVM) algorithms for the two separate classification tasks. The first task aims to classify vegetation cover into four classes using NDVI, GNDVI, and EVI spectral indices. The second task involves classifying burn severity into four classes using NBR, dNBR, and MIRBI spectral indices. 80% of the 1,000 random samples are used for training the classifiers, while the remaining 20% are used as test samples for evaluating their performance.

3.5 Hyperparameter Tuning

Hyperparameter tuning plays a crucial role in the training process and significantly impacts the final results to improve the classification accuracy results (Manafifard, 2024). Although many hyperparameters for commonly used classification algorithms in GEE are set to default values and do not require manual adjustment, a grid search approach was employed to achieve more accurate results in the classifications performed by the KNN, RF, GBDT, and SVM classifiers. The K value for the KNN, the number of trees for the RF and GBDT, and the C value for SVM were identified as key hyperparameters. The grid search approach was employed within a restricted search space to find the best values for these hyperparameters, which improved the results' accuracy.

3.6 Decision-Level Fusion (Late Fusion)

Decision-Level Fusion, also known as Late Fusion, integrates the results obtained from the classifications performed by the KNN, RF, GBDT, and SVM classifiers. Decision-level fusion involves combining the outputs of multiple independent models after the classification process has been completed to derive a final decision with enhanced accuracy and reliability. Late fusion facilitates more robust decision-making by synthesizing the final outputs of different classifiers (Le Bris et al., 2019). Among the various decision-level fusion methods, the accuracy-based weighting technique was chosen to integrate the classification results for this study. In this technique, the

classification results are weighted based on the overall accuracy rates of the classifiers to ensure a more precise final classification. In other words, more accurate classifications have a greater influence on the final result. This approach was applied to the vegetation cover and burn severity classifications performed by the KNN, RF, GDBT, and SVM classifiers. To apply decision-level fusion with a weighting approach based on accuracy, the sum of the accuracies of the classifications must equal 1 or 100%. Since the sum of the multiple classifications accuracies typically exceeds this value, it is necessary to normalize the accuracy of all classifications to be considered their effective weight. To do this, the overall accuracy rate of each classification is divided by the sum of the overall accuracy rates of all classifications to calculate the normalized weight.

3.7 Burned Vegetation Detection

In the final step, to assess post-wildfire burned vegetation, it is necessary to distinguish burned vegetation pixels from other burned surface features pixels, such as soil, so that the focus can be on burned vegetation. The results of both fused vegetation cover and burn severity classifications were overlaid for burned vegetation detection. Vegetation pixels in vegetation cover classification that overlapped with burned pixels were considered burned vegetation, while the remaining pixels that did not meet this criterion were considered unburned vegetation and other surface features.

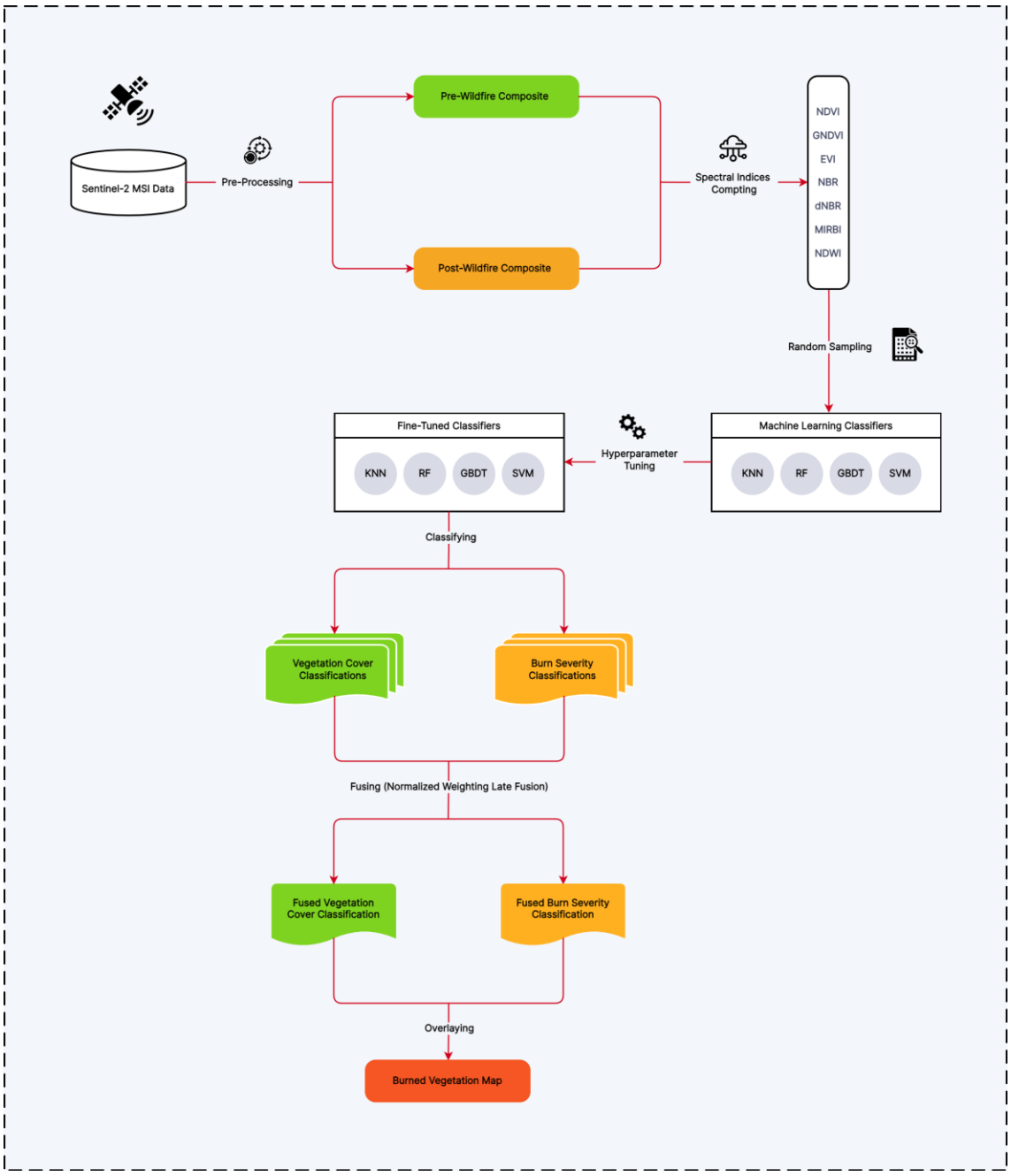

Figure 3. Methodology flowchart.

4. Results

4.1 Fine-Tuned Classifiers Evaluation

After hyperparameters tuning through Grid Search, the fine-tuned classifiers achieved overall accuracies of 97.36%, 99.45%, 97.95%, and 98.53% for vegetation cover classification and 98.08%, 94.79%, 92.38%, and 98.16% for burn severity classification, respectively. Figure 5 shows the accuracy progression of the classifiers for vegetation cover and burn severity classification tasks during the hyperparameter tuning process, demonstrating how the models' performance improved as best hyperparameters were identified. The KNN classifier experienced a decrease in overall accuracy after reaching its peak as the K value increased. Therefore, KNN performed better with a lower K value. In contrast, the overall accuracy of the RF and GBDT classifiers improved with the exponential increase in the number of trees. The SVM classifier achieved higher accuracies as the value of the C parameter increased. The kernel type in the SVM classifier was consistently set to RBF in all iterations.

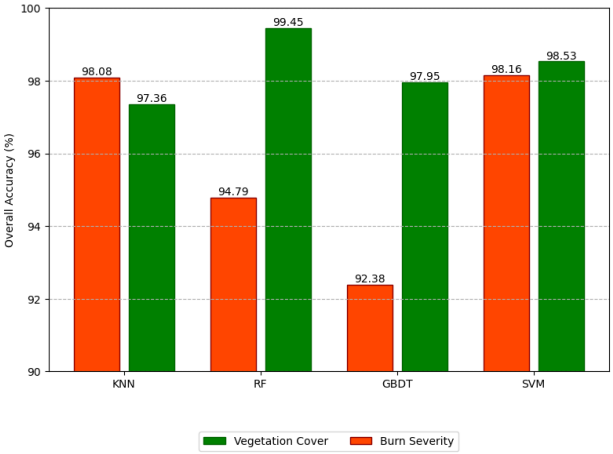

Figure 4. Classifiers' overall accuracies.

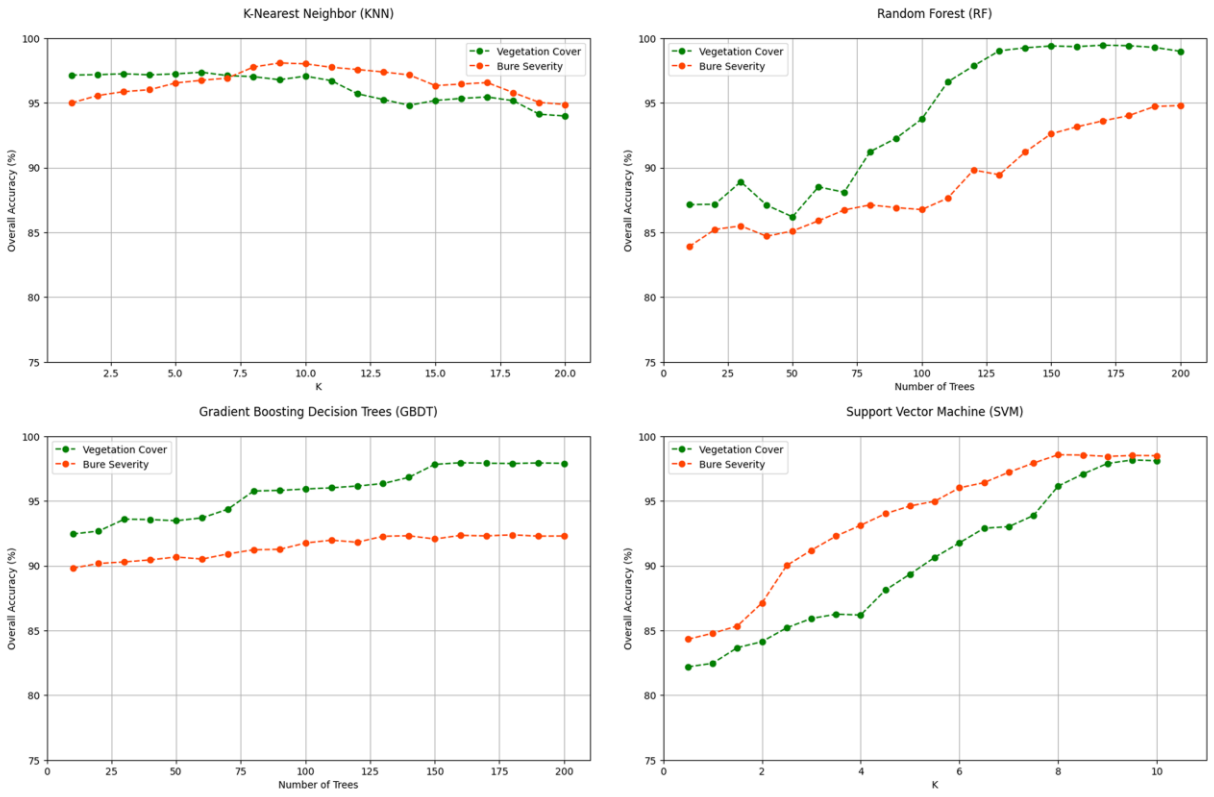

Figure 5. Classifiers' hyperparameter tuning.

4.2 Normalized Weights

These values were calculated by dividing the overall accuracy of each classifier by the sum of the accuracies of all the classifiers. In Equation 1, the normalized weight for vegetation cover classification using the KNN classifier model is calculated;

$$KNN\ Normalized\ Weight = \frac{A_1}{A_1 + A_2 + A_3 + A_4} = \frac{0.9736}{0.9736 + 0.9945 + 0.9795 + 0.9853} = 0.3239 \quad (1)$$

where A_1 = KNN overall accuracy rate
A_2 = RF overall accuracy rate
A_3 = GBDT overall accuracy rate
A_4 = SVM overall accuracy rate

Therefore, the KNN classifier played a 41% role in the fused vegetation cover classification. Table 2 shows the normalized weights based on the fine-tuned classifiers.

Classifier	Classification	Normalized Weight
KNN	Vegetation Cover	0.2475
RF	Vegetation Cover	0.2529
GBDT	Vegetation Cover	0.2490
SVM	Vegetation Cover	0.2505
KNN	Burn Severity	0.2580
RF	Burn Severity	0.2472
GBDT	Burn Severity	0.2409
SVM	Burn Severity	0.2560

Table 2. Calculated normalized weights

4.3 Fused Classifications

After determining the contribution of each classification result through the calculation of normalized weights, these results were fused to generate the final vegetation cover and burn severity classifications. Figure 4 shows these fused classifications. The vegetation cover classification includes Non-Vegetated, Low Vegetation, Moderate Vegetation, and Dense Vegetation classes. Surface features such as rocks, bare soil, river sands, built-up, and water bodies are all classified under the Non-Vegetated class.

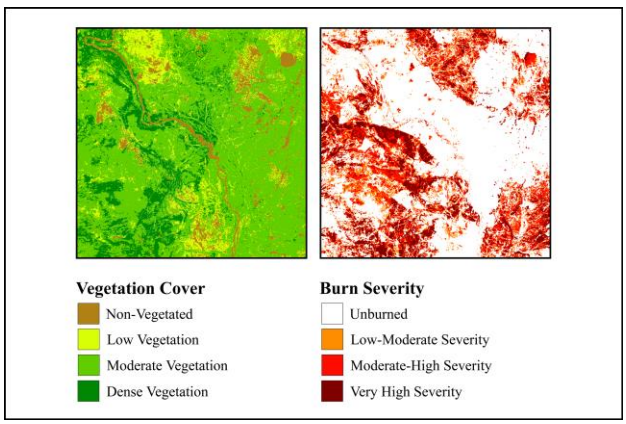

Figure 6. Fused classifications.

Vegetation, such as grasslands, shrubs, forests, etc, is also classified into the remaining three classes based on the density level and sensitivity to chlorophyll. Table 3 presents the calculated area for the vegetation cover classes.

ID	Class	Coverage Area (km^2)
1	Non-Vegetation	1437.472
2	Low Vegetation	1691.852
3	Moderate Vegetation	6554.430
4	Dense Vegetation	2554.207
-	Total Vegetation Cover Area	10800.489

Table 3. Calculated area of vegetation cover.

All burned surface features are classified based on burn severity, and burn severity is classified into Unburned, Low-Moderate Severity, Moderate-High Severity, and Very High Severity classes. This classification includes burned vegetation and other burned surface features such as bare soil and built-up. Table 4 presents the calculated area for burn severity classes.

ID	Class	Coverage Area (km^2)
1	Unburned	7569.291
2	Low-Moderate Severity	1117.502
3	Moderate-High Severity	1832.028
4	Very high Severity	1539.864
-	Total Burned Area	4489.394

Table 4. Calculated area of burn severity.

4.4 Detected Burned Vegetation

Figure 7 shows the pixels detected as burned vegetation after overlapping the fused vegetation cover and burn severity classifications. This figure does not include other burned surface features such as soil, rocks, river sands, and built-up.

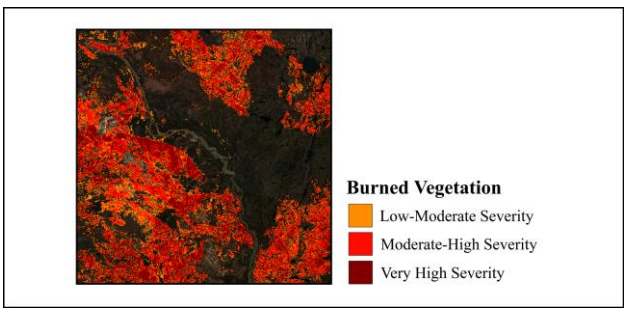

Figure 7. Detected burned vegetation visualization.

The total area of post-wildfire burned vegetation is obtained by calculating the total area of these pixels. Table 4 presents the calculated area of burned vegetation.

ID	Class	Coverage Area (km^2)
1	Low-Moderate Severity	991.756
2	Moderate-High Severity	1663.941
3	Very high Severity	1432.582
-	Total Burned Vegetation Area	4088.279

Table 4. Calculated area of burned vegetation.

Furthermore, a final map is generated by overlaying the burned vegetation pixels, vegetation classification classes, and water bodies extracted using the NDWI index. The final map provides a more comprehensive visual understanding of the extent of the damage caused by the wildfire. Figure 8 shows the final map.

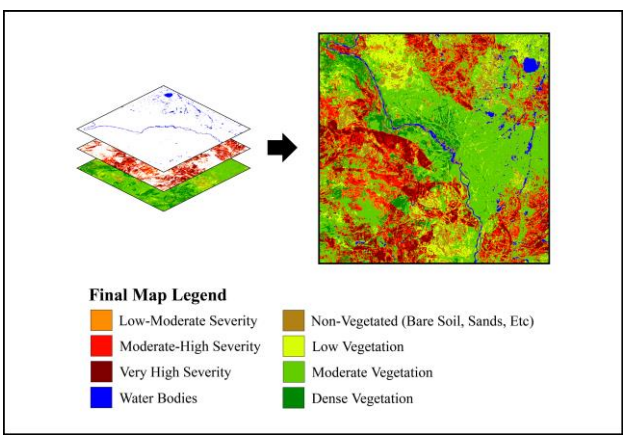

Figure 8. Final map.

https://doi.org/10.5194/isprs-archives-XLVIII-3-W3-2024-45-2024 | © Author(s) 2024. CC BY 4.0 License.

Based on the information provided in Tables 3, 4, and 5, the vegetation cover of the study area was 10,766.754 km^2, of which 4,087.765 km^2 were burned after the wildfire events. In other words, out of the total burned area of 4,489.394 km^2, which includes all burned surface features, only 4088.279 km^2 burned was vegetation cover. This accounts for 34.06% of the entire study area and 91.06% of the affected burned area. Therefore, the vegetation in this area has sustained significant damage following the wildfire.

5. Discussion

This study demonstrates that using Sentinel-2 MSI data and processing them on the GEE platform can aid in rapidly and accurately assessing burned vegetation following a wildfire. The KNN, RF, GBDT, and SVM classifiers, trained using random samples from the NDVI, GNDVI, and EVI spectral indices, effectively classified pre-fire vegetation and post-fire burn severity. Utilizing different vegetation indices for examination and classification can enhance the accuracy of the results, as each spectral index, due to its unique structure and use of different spectral bands, can yield distinct results. Consequently, integrating these results with methods like machine learning, as used in this study, can lead to more precise analysis. Additionally, Fusing the classification results from different classifiers through decision-level fusion resulted in a more comprehensive outcome, as the advantages of all three machine learning algorithms were leveraged. Moreover, using the GEE has enabled faster and more efficient data processing. This is particularly important in emergencies such as large wildfires requiring rapid and accurate assessment. Overcoming hardware limitations due to cloud-based processing is another advantage of this platform.

6. Conclusion

Wildfires are among the most destructive natural events, capable of causing significant damage to ecosystems, particularly the vegetation of a region. In some parts of the world, the frequency of large wildfires is higher than in other areas; an example of this can be seen in Canada's forests and grasslands. Fortunately, with advancements in remote sensing satellites and the increased diversity and capabilities of these technologies, it has become increasingly possible to monitor and manage wildfires, assess damages, and even predict them to a large extent. This allows affected and threatened communities to respond more effectively to such incidents. Among free multispectral data sources such as Sentinel-2, Landsat series, and MODIS, utilizing Sentinel-2 data can enhance the accuracy of classification results and provide more precise assessments of burned areas compared to Landsat and MODIS data, which have lower spatial resolution.

In this study, Sentinel-2 MSI data effectively demonstrated the damage to vegetation cover following the wildfires. The high accuracy of the machine learning models, which classified vegetation cover and burn severity, was achieved using spectral indices such as NDVI, GNDVI, EVI, NBR, dNBR, and MIRBI, each with different sensitivities to features. Applying a decision-level fusion approach combined these classification results to enhance the more accurate final result. This study revealed that the 2023 Canada Wildfires significantly damaged the study area's vegetation cover, represented by just one Sentinel-2 imagery tile. Over 90% of the burned areas consisted of burned vegetation. This result indicates that the damage across different regions of Canada after the wildfires must be far more devastating. It is recommended that future research explore more applications of this method in other areas and under various climatic conditions. The results of this study can aid in management decision-making and future planning to mitigate the negative impacts of wildfires and even assist in planning the recovery and restoration of burned vegetation areas. Additionally, using more advanced machine learning techniques and higher spatial resolution satellite imagery data can help improve the assessment accuracy. Investigating the long-term impacts of wildfires on vegetation cover and its recovery is also an important research avenue.

References

Aksoy, B., Çakmak, B., Kumbasar, N. 2023. Muğla Wildfires Burn Severity and Vegetation Difference Analysis with Remote Sensing Techniques. In *2023 31st Signal Processing and Communications Applications Conference*, pp. 1-4.

Amos, C., Petropoulos, G. P., Ferentinos, K. P. 2019. Determining the use of Sentinel-2A MSI for wildfire burning and severity detection. *International journal of remote sensing*, 40(3), 905-930.

Badda, H., Cherif, E. K., Boulaassal, H., Wahbi, M., Yazidi Alaoui, O., Maatouk, M., El Kharki, O. 2023. Improving the Accuracy of Random Forest Classifier for Identifying Burned Areas in the Tangier-Tetouan-Al Hoceima Region Using Google Earth Engine. *Remote Sensing*, 15(17), 4226.

Bastarrika, A., Chuvieco, E., Martín, M. P. 2011. Mapping burned areas from Landsat TM/ETM+ data with a two-phase algorithm: Balancing omission and commission errors. *Remote Sensing of Environment*, 115(4), 1003-1012.

Breiman, L. 2001. Random forests. *Machine learning*, 45, 5-32.

Brovelli, M. A., Sun, Y., Yordanov, V. 2020. Monitoring forest change in the amazon using multi-temporal remote sensing data and machine learning classification on Google Earth Engine. *ISPRS International Journal of Geo-Information*, 9(10), 580.

Claverie, M., Ju, J., Masek, J. G., Dungan, J. L., Vermote, E. F., Roger, J. C., Justice, C. 2018. The Harmonized Landsat and Sentinel-2 surface reflectance data set. *Remote Sensing of Environment*, 219, 145-161.

Chuvieco, E., Aguado, I., Salas, J., García, M., Yebra, M., Oliva, P. 2020. Satellite remote sensing contributions to wildland fire science and management. *Current Forestry Reports*, 6, 81-96.

Drusch, M., Del Bello, U., Carlier, S., Colin, O., Fernandez, V., Gascon, F., Bargellini, P. 2012. Sentinel-2: ESA's optical high-resolution mission for GMES operational services. *Remote Sensing of Environment*, 120, 25-36.

Zúñiga Espinoza, C., Khot, L. R., Sankaran, S., Jacoby, P. W. 2017. High resolution multispectral and thermal remote sensing-based water stress assessment in subsurface irrigated grapevines. *Remote Sensing*, 9(9), 961.

Fassnacht, F. E., Schmidt-Riese, E., Kattenborn, T., Hernández, J. 2021. Explaining Sentinel 2-based dNBR and RdNBR variability with reference data from the bird's eye (UAS) perspective. *International Journal of Applied Earth Observation and Geoinformation*, 95, 102262.

French, N. H., Kasischke, E. S., Hall, R. J., Murphy, K. A., Verbyla, D. L., Hoy, E. E., Allen, J. L. 2008. Using Landsat data to assess fire and burn severity in the North American boreal forest region: an overview and summary of results. *International Journal of Wildland Fire*, 17(4), 443-462.

Gemitzi, A., Koutsias, N. 2022. A Google Earth Engine code to estimate properties of vegetation phenology in fire affected areas–A case study in North Evia wildfire event on August 2021. *Remote Sensing Applications: Society and Environment*, 26, 100720.

Gibson, R., Danaher, T., Hehir, W., Collins, L. 2020. A remote sensing approach to mapping fire severity in south-eastern Australia using sentinel 2 and random forest. *Remote Sensing of Environment*, 240, 111702.

Gholamrezaie, H., Hasanlou, M., Amani, M., Mirmazloumi, S. M. 2022. Automatic mapping of burned areas using Landsat 8 time-series images in Google Earth engine: A case study from Iran. *Remote Sensing*, 14(24), 6376.

Gorelick, N., Hancher, M., Dixon, M., Ilyushchenko, S., Thau, D., Moore, R. 2017. Google Earth Engine: Planetary-scale geospatial analysis for everyone. *Remote Sensing of Environment*, 202, 18-27.

Huang, S., Tang, L., Hupy, J. P., Wang, Y., Shao, G. 2021. A commentary review on the use of normalized difference vegetation index (NDVI) in the era of popular remote sensing. *Journal of Forestry Research*, 32(1), 1-6.

Hudak, A. T., Brockett, B. H. 2004. Mapping fire scars in a southern African savannah using Landsat imagery. *International Journal of Remote Sensing*, 25(16), 3231-3243.

Huot, F., Hu, R. L., Goyal, N., Sankar, T., Ihme, M., Chen, Y. F. 2022. Next day wildfire spread: A machine learning dataset to predict wildfire spreading from remote-sensing data. *IEEE Transactions on Geoscience and Remote Sensing*, 60, 1-13.

Ismailoglu, I., Musaoglu, N. 2023. Burn severity assessment with different remote sensing products for wildfire damage analysis. In *Earth Observing Systems* XXVIII, Vol. 12685, pp. 220-226.

Izadi, M., Mohammadzadeh, A., Haghighattalab, A. 2017. A new neuro-fuzzy approach for post-earthquake road damage assessment using GA and SVM classification from QuickBird satellite images. *Journal of the Indian Society of Remote Sensing*, 45, 965-977.

Jain, P., Barber, Q. E., Taylor, S., Whitman, E., Acuna, D. C., Boulanger, Y., Parisien, M. A. 2024. Canada Under Fire–Drivers and Impacts of the Record-Breaking 2023 Wildfire Season. *Authorea Preprints*.

Kalantar, B., Ueda, N., Idrees, M. O., Janizadeh, S., Ahmadi, K., Shabani, F. 2020. Forest fire susceptibility prediction based on machine learning models with resampling algorithms on remote sensing data. *Remote Sensing*, 12(22), 3682.

Kolden, C. A., Abatzoglou, J. T., Jones, M. W., Jain, P. 2024. Wildfires in 2023. *Nature Reviews Earth and Environment*, 5(4), 238-240.

Kulinan, A. S., Cho, Y., Park, M., Park, S. 2024. Rapid wildfire damage estimation using integrated object-based classification with auto-generated training samples from Sentinel-2 imagery on Google Earth Engine. *International Journal of Applied Earth Observation and Geoinformation*, 126, 103628.

Leblon, B. 2001. Forest wildfire hazard monitoring using remote sensing: A review. *Remote Sensing Reviews*, 20(1), 1-43.

Le Bris, A., Chehata, N., Ouerghemmi, W., Wendl, C., Postadjian, T., Puissant, A., Mallet, C. 2019. Decision fusion of remote-sensing data for land cover classification. In *Multimodal Scene Understanding*, pp. 341-382.

Lee, K., van Leeuwen, W. J., Gillan, J. K., Falk, D. A. 2024. Examining the Impacts of Pre-Fire Forest Conditions on Burn Severity Using Multiple *Remote Sensing Platforms. Remote Sensing*, 16(10), 1803.

Liu, S., Qiu, J., Li, F. 2024. A Remote Sensing Water Information Extraction Method Based on Unsupervised Form Using Probability Function to Describe the Frequency Histogram of NDWI: A Case Study of Qinghai Lake in China. *Water*, 16(12), 1755.

Loboda, T., O'neal, K. J., Csiszar, I. 2007. Regionally adaptable dNBR-based algorithm for burned area mapping from MODIS data. *Remote Sensing of Environment*, 109(4), 429-442.

Long TengFei, L. T., Zhang ZhaoMing, Z. Z., He GuoJin, H. G., Jiao WeiLi, J. W., Tang Chao, T. C., Wu BingFang, W. B., Yin RanYu, Y. R. 2019. 30 m resolution global annual Burned Area mapping based on Landsat images and Google Earth Engine. *Remote Sensing*, 11(5), 489.

Ahmed, S. A., N, H. 2023. Land use and land cover classification using machine learning algorithms in google earth engine. *Earth Science Informatics*, 16(4), 3057-3073.

Manafifard, M. 2024. A new hyperparameter to random forest: application of remote sensing in yield prediction. *Earth Science Informatics*, 17(1), 63-73.

Mandanici, E., Bitelli, G. 2016. Preliminary comparison of sentinel-2 and landsat 8 imagery for a combined use. *Remote Sensing*, 8(12), 1014.

Mutanga, O., Kumar, L. 2019. Google earth engine applications. *Remote Sensing*, 11(5), 591.

Pacheco, A. D. P., Junior, J. A. D. S., Ruiz-Armenteros, A. M., Henriques, R. F. F. 2021. Assessment of k-nearest neighbor and random forest classifiers for mapping forest fire areas in central portugal using landsat-8, sentinel-2, and terra imagery. *Remote Sensing*, 13(7), 1345.

Palandjian, D., Gitas, I. Z., Wright, R. 2009. Burned area mapping and post-fire impact assessment in the Kassandra peninsula (Greece) using Landsat TM and Quickbird data. *Geocarto International*, 24(3), 193-205.

Pérez, C. C., Olthoff, A. E., Hernández-Trejo, H., Rullán-Silva, C. D. 2022. Evaluating the best spectral indices for burned areas in the tropical Pantanos de Centla Biosphere Reserve, Southeastern Mexico. *Remote Sensing Applications: Society and Environment*, 25, 100664.

Pérez-Cabello, F., Montorio, R., Alves, D. B. 2021. Remote sensing techniques to assess post-fire vegetation recovery. *Current Opinion in Environmental Science and Health*, 21, 100251.

Petropoulos, G. P., Griffiths, H. M., Kalivas, D. P. 2014. Quantifying spatial and temporal vegetation recovery dynamics following a wildfire event in a Mediterranean landscape using EO data and GIS. *Applied Geography*, 50, 120-131.

Prasad, A. D., Ganasala, P., Hernández-Guzmán, R., Fathian, F. 2022. Remote sensing satellite data and spectral indices: an initial evaluation for the sustainable development of an urban area. *Sustainable Water Resources Management*, 8(1), 19.

Priya, R. S., Vani, K. 2024. Vegetation change detection and recovery assessment based on post-fire satellite imagery using deep learning. *Scientific Reports*, 14(1), 12611.

Rao, H., Shi, X., Rodrigue, A. K., Feng, J., Xia, Y., Elhoseny, M., Gu, L. 2019. Feature selection based on artificial bee colony and gradient boosting decision tree. *Applied Soft Computing*, 74, 634-642.

Salvoldi, M., Siaki, G., Sprintsin, M., Karnieli, A. 2020. Burned area mapping using multi-temporal sentinel-2 data by applying the relative differenced aerosol-free vegetation index (RdAFRI). *Remote Sensing*, 12(17), 2753.

Seydi, S. T., Akhoondzadeh, M., Amani, M., Mahdavi, S. 2021. Wildfire damage assessment over Australia using sentinel-2 imagery and MODIS land cover product within the google earth engine cloud platform. *Remote Sensing*, 13(2), 220.

Sobrino, J. A., Llorens, R., Fernández, C., Fernández-Alonso, J. M., Vega, J. A. 2019. Relationship between soil burn severity in forest fires measured in situ and through spectral indices of remote detection. *Forests*, 10(5), 457.

Son, N. T., Chen, C. F., Chen, C. R., Minh, V. Q., Trung, N. H. 2014. A comparative analysis of multitemporal MODIS EVI and NDVI data for large-scale rice yield estimation. *Agricultural and Forest Meteorology*, 197, 52-64.

Song, X. P., Huang, W., Hansen, M. C., Potapov, P. 2021. An evaluation of Landsat, Sentinel-2, Sentinel-1 and MODIS data for crop type mapping. *Science of Remote Sensing*, 3, 100018.

Soverel, N. O., Perrakis, D. D., Coops, N. C. 2010. Estimating burn severity from Landsat dNBR and RdNBR indices across western Canada. *Remote Sensing of Environment*, 114(9), 1896-1909.

Srivastava, S., Senthil Kumar, A. 2020. Implications of intense biomass burning over Uttarakhand in April–May 2016. *Natural Hazards*, 101, 367-383.

Vandansambuu, B., Gantumur, B., Wu, F., Byambasuren, O., Bayarsaikhan, S., Chantsal, N., Jimseekhuu, M. E. 2023. Assessment of burn severity and monitoring of the wildfire recovery process in Mongolia. *Fire*, 6(10), 373.

Veraverbeke, S., Verstraeten, W. W., Lhermitte, S., Goossens, R. 2010. Evaluating Landsat Thematic Mapper spectral indices for estimating burn severity of the 2007 Peloponnese wildfires in Greece. *International Journal of Wildland Fire*, 19(5), 558-569.

Veraverbeke, S., Harris, S., Hook, S. 2011. Evaluating spectral indices for burned area discrimination using MODIS/ASTER (MASTER) airborne simulator data. *Remote Sensing of Environment*, 115(10), 2702-2709.

Wang, J., Zhang, X. 2020. Investigation of wildfire impacts on land surface phenology from MODIS time series in the western US forests. *ISPRS Journal of Photogrammetry and Remote Sensing*, 159, 281-295.

Wang, Q., Blackburn, G. A., Onojeghuo, A. O., Dash, J., Zhou, L., Zhang, Y., Atkinson, P. M. 2017. Fusion of Landsat 8 OLI and Sentinel-2 MSI data. *IEEE Transactions on Geoscience and Remote Sensing*, 55(7), 3885–3899.

Zidane, I. E., Lhissou, R., Ismaili, M., Manyari, Y., Bouli, A., Mabrouki, M. 2021. Characterization of fire severity in the Moroccan rif using Landsat-8 and Sentinel-2 satellite images. *Int. J. Adv. Sci. Eng. Inf. Technol*, 11, 72-83.